MoO_3 films grown on polycrystalline Cu: Morphological, structural, and electronic properties

Salvatore Macis, Carla Aramo, Carmela Bonavolontà, Giannantonio Cibin, Alessandro D'Elia, Ivan Davoli, Mario De Lucia, Massimiliano Lucci, Stefano Lupi, Marco Miliucci, Andrea Notargiacomo, Carlo Ottaviani, Claudio Quaresima, Manuela Scarselli, Jessica Scifo, Massimo Valentino, Paola De Padova, and Augusto Marcelli

Citation: Journal of Vacuum Science & Technology A **37**, 021513 (2019); doi: 10.1116/1.5078794
View online: https://doi.org/10.1116/1.5078794
View Table of Contents: https://avs.scitation.org/toc/jva/37/2
Published by the American Vacuum Society

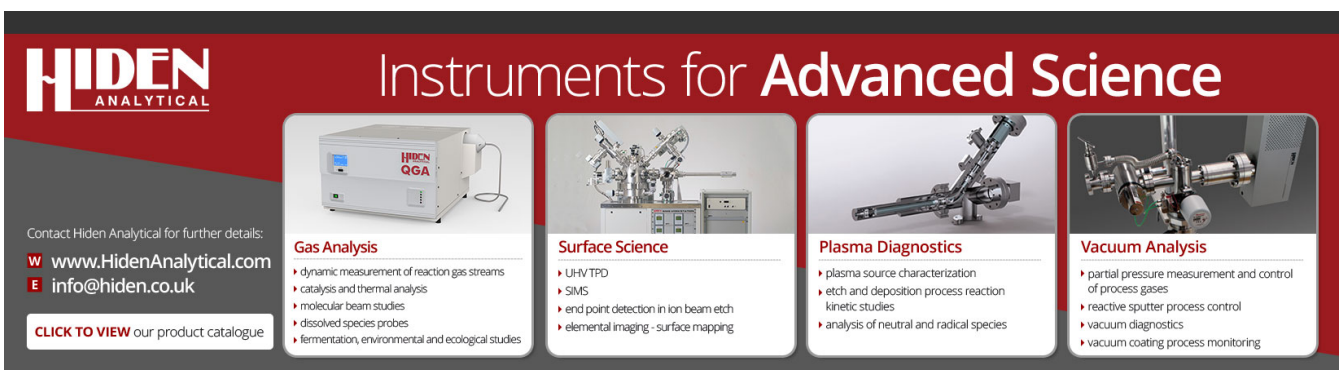

MoO_3 films grown on polycrystalline Cu: Morphological, structural, and electronic properties

Salvatore Macis,[1,2,a] Carla Aramo,[3] Carmela Bonavolontà,[3] Giannantonio Cibin,[4] Alessandro D'Elia,[5] Ivan Davoli,[1,2] Mario De Lucia,[3] Massimiliano Lucci,[1] Stefano Lupi,[6] Marco Miliucci,[2] Andrea Notargiacomo,[7] Carlo Ottaviani,[8] Claudio Quaresima,[8] Manuela Scarselli,[9] Jessica Scifo,[2] Massimo Valentino,[3,10] Paola De Padova,[8] and Augusto Marcelli[2,11]

[1]*Department of Physics, Università di Roma Tor Vergata, via della Ricerca Scientifica 1, 00133 Rome, Italy*
[2]*INFN, Laboratori Nazionali di Frascati, via Enrico Fermi 40, 00044 Frascati, Italy*
[3]*INFN, Sezione di Napoli, Via Cintia 2, 80126 Napoli, Italy*
[4]*Diamond Light Source, Harwell Science and Innovation Campus, Didcot OX11 0DE, UK*
[5]*Department of Physics, University of Trieste, 34127 Trieste, Italy*
[6]*Department of Physics, Università di Roma La Sapienza, Piazzale Aldo Moro 5, 00185 Rome, Italy*
[7]*CNR—Istituto di Fotonica e Nanotecnologie, via Cineto Romano, 42, 00156 Roma, Italy*
[8]*CNR-ISM, Via del Fosso del Cavaliere, 100, 00133 Roma, Italy*
[9]*Department of Physics, Università di Roma Tor Vergata, and INFN sezione Tor Vergata, via della Ricerca Scientifica 1, 00133 Rome, Italy*
[10]*CNR-ISASI, via Campi Flegrei 34, 80078 Pozzuoli, Italy*
[11]*Rome International Centre for Material Science Superstripes, RICMASS, via dei Sabelli 119A, 00185 Rome, Italy*

(Received 29 October 2018; accepted 18 January 2019; published 8 February 2019)

In this work, the authors investigated MoO_3 films with thickness between 30 nm and 1 μm grown at room temperature by solid phase deposition on polycrystalline Cu substrates. Atomic force microscopy, scanning electron microscopy, and scanning tunneling microscopy revealed the presence of a homogenous MoO_3 film with a "grainlike" morphology, while Raman spectroscopy showed an amorphous character of the film. Nanoindentation measurements evidenced a coating hardness and stiffness comparable with the copper substrate ones, while Auger electron spectroscopy, x-ray absorption spectroscopy, and secondary electron spectroscopy displayed a pure MoO_3 stoichiometry and a work function $\Phi_{MoO3} = 6.5$ eV, 1.8 eV higher than that of the Cu substrate. MoO_3 films of thickness between 30 and 300 nm evidenced a metallic behavior, whereas for higher thickness, the resistance–temperature curves showed a semiconducting character. *Published by the AVS.* https://doi.org/10.1116/1.5078794

I. INTRODUCTION

Transition metal (TM) oxides are systems extremely interesting for both fundamental and technological issues. They exhibit a richness of electronic and magnetic physical properties, such as metal–insulator transition,[1] colossal magnetoresistance,[2] and high temperature superconductivity,[3] mainly originated from their wide range of structures joined to the electronic configurations of their outer *d* states, which is a seed of strong electron correlation behavior.[4]

TM oxides are important for several technological applications, namely, in microelectronic devices, sensors, and catalysis processes.[5,6] As an example, low-cost hydrogen-doped molybdenum oxides with the morphology of 2D nanodisks were recently used as ultrasensitive plasmonic biosensors with fast kinetics.[7] MoO_3 can also be used to synthesize molybdenum sulfides, an emerging class of inorganic coordination polymers utilized for their superior catalytic properties. Indeed, MoS_x can be used to develop an electrolyteless water splitting photocatalyst, and their study have significant implications to the field of hydrogen evolution catalysis.[8] In addition to the above, molybdenum oxides are used in a huge number of industrial physical/chemical processes,[9] and in many of these applications, they are involved in surface charge exchange phenomena upon interface formation, a critical matter that strongly depends on materials work function (WF).

The work function of elemental metals typically ranges from a minimum value of 2.14 eV for Cs to a maximum value of 5.65 eV for Pt,[10] whereas copper surfaces have a WF value between 4.5 and 5.1 eV. The possibility that metallic materials could have a WF significantly higher than Pt is very important for technological applications. The TM oxide WF can range from extremely low values, e.g., ~3 eV as for ZrO_2,[11] to values up to ~7 eV such as in V_2O_5.[12] In addition to high WF values, the TM oxides' inorganic systems, such as MoO_3 (WF = 6.5–6.9 eV),[13] WO_3 (WF = 5–6.4 eV),[14] CrO_3 (WF = 6.9 eV),[13] and V_2O_5 (WF = 7 eV),[12] are semiconductors with a wide bandgap that can be easily degenerately doped by defects, modifying their transport properties.

At ambient conditions, MoO_3 exhibits three polymorphs: orthorhombic (α-MoO_3; Pbmn), hexagonal (h-MoO_3), and monoclinic (β-MoO_3; P21/n) phases. Among these three phases, only α-MoO_3 has a thermodynamically stable layered structure.[15,16] This layered phase contains Mo in distorted

Note: This paper is part of the Special Topic Collection on Complex Oxides.
[a]Electronic mail: salvatore.macis@roma2.infn.it

octahedral sites, and the edges of the Mo-O layers are terminated by nonbridging O1 sites.[15] Its high work function probably arises from dipoles originating by the terminal O1 sites lying outside the top layers. Due to its closed shell character as well as the dipoles created by its internal layer structure, MoO_3 is a high electron affinity oxide, which exhibits interesting conductivity features due to O vacancy formed by the partial reduction of Mo ions.[17] Naouel *et al.* discussed, in particular, the electrical properties of ordered layered α-MoO_3 nanosheets.[18] Actually, many aspects of the physics and chemistry of molybdenum oxides have recently been investigated, in particular, plasmonic contributions. However, many properties of bidimensional molybdenum oxide systems and quantum dots molybdenum oxides are still unknown and many research published still require a deeper understanding.[19]

A minimum thickness is needed to tune the conductivity of molybdenum oxides in contact with a metal such as copper via the band energy-level alignment with the interface. Recently, Greiner *et al.*[13] demonstrated how different TM oxide/metal interfaces could modify the original WF of the TM oxide and its electronic band structure. In particular, they focused on the d_0 oxide MoO_3, having an empty Mo 4*d*-band and a valence band mainly composed of O 2*p* states[20] with an $E_{gap} = 3.0–3.1$ eV. Its electronic band structure is highly dependent on the molybdenum oxidation state, which in stoichiometric MoO_3 is Mo^{6+}. However, defects mainly due to oxygen vacancies generate Mo^{5+} cations, which induce a partially occupied Mo 4*d*-band. Even "stoichiometric" MoO_3 is an n-type material with an equilibrium concentration of defects, but a continuous removal of oxygen may reduce MoO_3 to MoO_2, the lowest stable molybdenum oxide, which contains Mo^{4+} cations that give rise to the partially filled *d*-band. Greiner *et al.*[13] also discussed how different metallic substrates might lead MoO_3 to a semimetallic phase with a lower work function. This is the result of the reduction of Mo at the metal/oxide interface, a mechanism that is a function of the TM oxide thickness, the metal reactivity, and mutual work function. At the metal interface, the reduction of Mo^{6+} to Mo^{5+} and/or Mo^{4+} forms gap states, which tune the conductivity of the Mo oxide. Increasing the distance from the interface, the oxide becomes more stoichiometric and insulating. Among TMs, molybdenum is one of the most reactive materials so that the Cu/MoO_3 interface appears to be a suitable option for many applications, including improving radio frequency (RF) devices loaded by high electric fields near their surface. In these devices, breakdown phenomena and the presence of high magnetic field induce an increasing temperature, causing severe surface damages.[21] These phenomena cast considerable demands on the materials used to manufacture any accelerating structure. In particular, they must have as good as possible electrical and thermal conductivities as pure oxygen-free electronic copper C10100 (Cu-OFE) successfully used at RT in most accelerator applications. However, looking at the future applications, i.e., RF devices with electric gradients much higher than the present components at RT, the requirements are close or superior to the fundamental limitations of pure copper. Therefore, new materials such as high conductivity copper alloys or copper coated with TM oxides have to be considered for building the next generation of particle accelerators. The current technology is based on copper resonant cavities, cooled to low temperatures to reach gradients from 100 up to 1000 MV/m.[21] Even at these values, almost all cavities start reaching the breakdown limits where destructive discharge phenomena occur.[22] In the last few decades, many research studies attempted to understand the dynamics that trigger or inhibit the breakdown phenomenon, but this remains an open problem far to be understood.[21,22]

Another problem affecting the behavior of a resonant cavity is the dark current, i.e., the electrons emitted by the metallic surfaces when a cavity is subjected to high electric fields. All RF structures exhibit dark current after breakdown, and emitted electrons interfere with the accelerated charges affecting the beam quality. In addition to beam perturbation, this emission mechanism increases the heating of the cavities and may trigger further breakdowns.[21–23]

As discussed above, MoO_3 on copper is a really interesting option, since a thin layer of "insulating" MoO_3 on a thick copper substrate is actually conductive, while its work function is higher than copper. Moreover, this film may also improve the flatness of the copper surface, reducing the presence of tips and defects in the surface. The latter are considered among the main reasons for the occurrence of breakdown.[22]

In this work, we studied the structural, morphological, and electronic properties of molybdenum trioxide films, grown at RT by solid phase evaporation, on polished polycrystalline Cu substrates, with thickness ranging from 30 nm up to 1 μm. Several techniques, such as Auger electron and secondary spectroscopy (AES), atomic force microscopy (AFM), scanning electron microscopy (SEM), scanning tunneling microscopy (STM), nanoindentation, x-ray diffraction (XRD), x-ray absorption (XAS) Raman spectroscopy, and resistivity measurements, were applied to get insights on TM oxide/Cu systems. The results showed that the MoO_3 films grown on the Cu substrates at RT are amorphous, presenting a weak film–substrate adhesion. The MoO_3 film morphology exhibits a uniform grainlike morphology with a mean diameter of 30–100 nm, with either a high work function of 6.5 eV or metallic behavior for film thicknesses from 30 to 300 nm.

II. EXPERIMENT

Figure 1 shows the growth setup of the MoO_3 films: (a) a dedicated evaporation high vacuum (HV) chamber (2×10^{-5} mbar base pressure) equipped with an MoO_3 solid phase evaporation source and a quartz microbalance for monitoring films thickness illustrated in (b) and (c) a picture of a set of MoO_3/Cu films. A fast load-lock system allows for air–HV rapid samples transfer.

Polished polycrystalline Cu substrates with a nominal roughness less than 30 nm are used for the MoO_3 films deposition at the Tor Vergata University (Rome, Italy). The substrates were cleaned first with dips in acetone and then

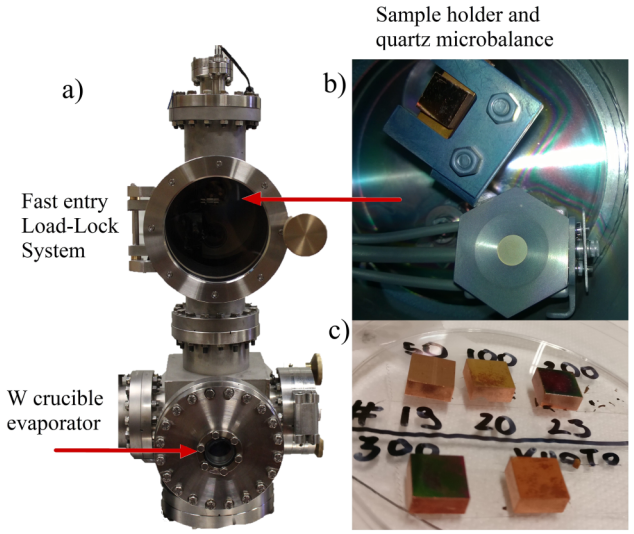

FIG. 1. Experimental setup of the MoO_3 growth apparatus: (a) the HV deposition chamber, where it is installed in the solid phase W-crucible MoO_3 source. The sample holder and quartz microbalance are illustrated in (b), while in (c) different MoO_3 films deposited on Cu substrates are showed.

sonicated for 5 min in 2-propanol, followed by a second sonication in ultrapure water for 10 min.

Pure MoO_3 (99.999%) powder from Sigma Aldrich was used to grow the TM oxide films, with a flux rate from 0.1 up to 2 Å/s. MoO_3 was placed into a tungsten crucible and evaporated at a temperature of 450–550 °C, keeping the Cu substrates at RT. The samples (maximum size of 200 mm, flat and/or with cylindrical curvature) were loaded in front of the MoO_3 evaporation source at a distance of ~400 mm, while a mechanical shutter allows one to open-and-close the evaporation flux. A quartz microbalance placed near the sample measures the films thickness [Fig. 1(b)].

SEM images were collected by means of MINI-SEM SNE-3200M with a magnification factor of up to 6×10,[4] operating at an accelerating voltage from 5 to 30 kV at INFN-LNF (Frascati, Italy), while STM was performed with the OMICRON system at the Tor Vergata University (Rome, Italy).

XAS experiments were performed at the B18 beamline at the Diamond Light Source (UK), while XRD experiments by using a Seifert MZ IV diffractometer with a Cu anode operating at 40 kV (30 mA) and an Ni filter in the $\theta - 2\theta$ Bragg-Brentano geometry at the INFN-LNF (Frascati, Italy).

AES and secondary electron spectroscopy were carried out at CNR-ISM (Rome, Italy) by means of a coaxial electron beam (Perkin-Elmer) double-pass cylindrical mirror electron analyzer, normally impinging on the surface samples. The used energy was $E_p = 1$ keV, $I \sim 10\,\mu$A, and modulation $V_{pp} = 2$ V. In order to reduce the MoO_3 electron bombardment damage, the energy electron beam was selected at $E_p = 1$ keV with a low filament current of $I \sim 10\,\mu$A.

Raman spectroscopy was carried out by a BW-TEK confocal microscope operating at wavelength $\lambda = 784.92$ nm ($P_{max} = 490$ mW, $\Delta E = \pm 1.5\,cm^{-1}$, and a laser spot of ~80 μm).

Nanoindentation measurements were performed at the Tor Vergata University (Rome, Italy) with the NanoTest™, MICRO MATERIALS, working with a round end cone tip of 25 μm diameter, performing multiple indentation cycles with submillinewton forces.

AFM images were obtained with a VEECO D3100 microscope equipped with the Nanoscope IIIa controller operated in Tapping Mode; silicon probes with 5–10 nm tip radius and 40 N m^{-1} nominal cantilever force constant were used.

STM imaging was performed under ultrahigh vacuum conditions (7.5×10^{-11} mbar) at room temperature (RT) using an Omicron-STM system (Omicron). Electrochemically etched tungsten tips (99.9% purity, Goodfellow GmbH) were used. All images were acquired in the constant current mode, and the collected data were unfiltered apart from rigid plane subtraction.

The resistivity measurements as a function of temperature from RT down to 20 K (±10 mK) were performed by a 3458A Agilent multimeter, at the INFN unit of Napoli (Italy), using an optical cryostat (Microstat Hires of Oxford Instruments®) equipped with a cold finger and monitored by the Intelligent Temperature Controller of Oxford Instruments. For electrical contact, two silver paint points were deposed on the film surface measuring the transversal resistance of the coatings. The error on the resistance measurement was less than 1% of the values.

III. RESULTS AND DISCUSSION

A. Morphology and mechanical properties: AFM, STM, SEM, and nanoindentation

The morphology and mechanical properties of molybdenum oxides films grown at RT on Cu substrates for two different thicknesses (30 and 100 nm) were studied by AFM, SEM, STM, and force nanoindentation.

The roughness of the copper substrate, as measured by the STM on an area as small as $2 \times 2\,\mu m^2$ [Fig. 2(a)], is ~7.4 nm. The average roughness on a 30 nm MoO_3 film (figure not shown), measured by STM, is ~4 nm.

Figure 2(b) shows a typical AFM morphology of a 100 nm thick MoO_3 film. The image points out a quite

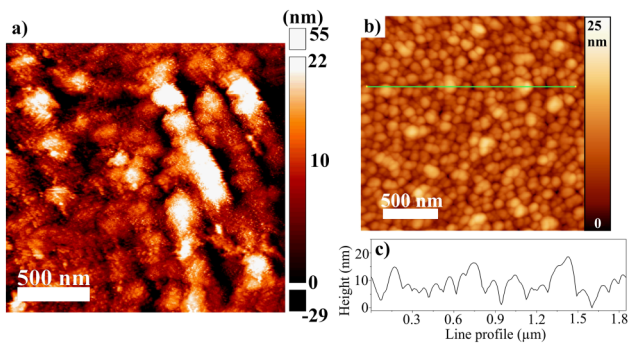

FIG. 2. (a) STM topography of a $2 \times 2\,\mu m^2$ of the Cu substrate with a measured roughness of ~7.4 nm: diagonal stripes are visible, probably due to the lapping procedure. (b) AFM image ($2 \times 2\,\mu m^2$) of the 100 nm thick MoO_3 film deposited on Cu (b). (c) height line profile along the horizontal trace drawn in panel (b).

homogeneous grainlike morphology with an average grain radius of 50 nm and an RMS roughness of 2.9 nm, which is in agreement with the value measured by STM. This grain size value is particularly important for technological properties, being slightly greater than the electron mean free path of copper (~40 nm). The height profile of Fig. 2(c) shows that the peak-valley excursion along the line on the AFM image (b) is below 15 nm.

These results point out that the average roughness of molybdenum oxide films can be smaller than polished copper, also for the lowest thickness of our films (~30 nm). This is an important result since the local surface roughness is a critical issue of RF accelerating components. Tips and roughness at the surface could trigger breakdown phenomena, compromising the operation of RF structures for which a high smooth surface is required. Figure 3 shows two SEM micrographs collected on the 100 nm MoO_3 film at a magnification of 60× (a) and 3000× (b). All samples showed a uniform coating with no evident grain growth at a micrometric scale [see Fig 3(a)]. In our MoO_3 films, the grain structures are not resolved by SEM measurements due to their high flatness. Nevertheless, on these films, it is possible to find areas with defects and regions where the coating does not perfectly adhere to the substrate [Fig. 3(b)]. The film adhesion on Cu substrates is an important challenge. It can be improved, as the structural, microstructural, and electrical behavior, by optimizing the growth parameters, in addition to the residual vacuum into the deposition apparatus.[24]

For many technological applications, the hardness of materials is another crucial property. As an example when a ductile metal-like copper is deformed plastically, the local change of shape at the microscopic scale is converted into dislocations and twinning, which may affect the hardness of the material. Moreover, the prevailing theory of RF breakdown physics points out that by increasing the material hardness, it is possible to improve the operational gradients of an accelerating structure. This is also confirmed by testing RF devices working at cryogenic temperatures.[25] Traditional microhardness tests involve applied loads and for most materials, the resultant indents are large enough to be observable by an optical microscope. Nanoindentation can involve applied loads in the sub-mN range so that the usual indent size is in the sub-μm range. It allows the load and displacement to be continuously monitored and recorded during the indentation process.

The load–displacement data produced well-controlled quantities such as hardness and elastic modulus from sub-μmmicron-sized indents. From the indentation data, we can obtain the average hardness value and the reduced modulus, i.e., to evaluate the stiffness of the material.

Figure 4 displays typical indentation hysteresis curves (load vs depth) of the Cu substrate and of a 100 nm MoO_3 film. For all films, multiple indentation cycles with millinewton and submillinewton forces were performed, and for each cycle, a hysteresis curve was recorded. The plastic deformation during the indentation is well evident from Fig. 4 where the two steps of the indentation process are shown. The first is when the tip perforates the surface (left arrow) to a maximum force of 3 mN, and the second part is when the tip is extracted (right arrow) leaving ~10 nm displacement due to the plastic deformation of the sample. The hardness ($\boldsymbol{H}$) measured from these hysteresis curves is defined as the maximum load $\boldsymbol{P}_{\max}$ divided by the residual indentation area $\boldsymbol{A_r}$. The setup measures the depth of penetration, which is used to determine the area $\boldsymbol{A_r}$ using the known shape of the diamond conical tip. The reduced modulus, $\boldsymbol{E_r}$, is a variation of the Young modulus, which defines the linear relation between stress and strain inside the material. $\boldsymbol{E_r}$ is calculated by analyzing the slope of the indentation hysteresis curves and the displacement due to the plastic deformation. Similar measurements were applied on polished polycrystalline Cu substrates. We report in Table I the hardness $\boldsymbol{H}$ and the reduced modulus $\boldsymbol{E_r}$ of the polycrystalline polished Cu substrate and of the three MoO_3 films with thicknesses of 100, 300, and 400 nm. Each $\boldsymbol{H}$ and $\boldsymbol{E_r}$ values are obtained by the average calculated on a set of 25 measurements. σ_H and σ_{Er} standard deviations are also reported.

Interestingly, as shown in Table I, within the uncertainty of these measurements, MoO_3 films grown at RT are characterized by values of hardness, $\boldsymbol{H}$, and reduced modulus, $\boldsymbol{E_r}$, very near to those of the Cu substrate. $\boldsymbol{H}$ and $\boldsymbol{E_r}$ of MoO_3

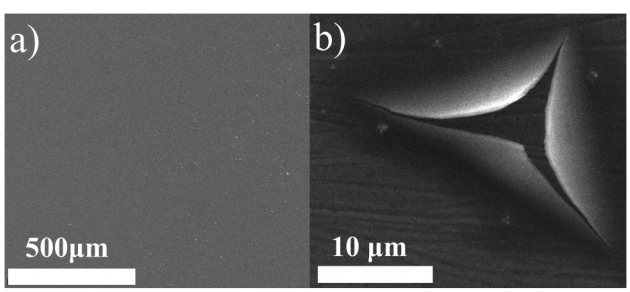

FIG. 3. SEM images from the 100 nm MoO_3 film on the copper substrate collected at 30 kV at a magnification of 60× (a) and 3000×. Panel (b) shows a region, where the film lost adhesion with the underneath Cu substrate

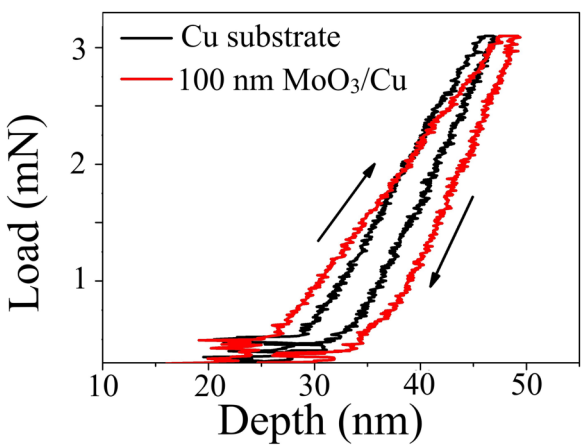

FIG. 4. Two typical load–depth hysteresis curves collected on the pristine Cu substrate and on the 100 nm thick MoO_3 film deposited on Cu. The arrows represent the up and down force cycle with the maximal force applied of 3 mN.

TABLE I. Hardness H and reduced modulus E_r of the copper substrate and different MoO_3/Cu films; σ_H and σ_{Er} are the standard deviations.

Sample	H (GPa)	σ_H (GPa)	E_r (GPa)	σ_{Er} (GPa)
Cu	1.43	0.26	134	18
100 nm MoO_3/Cu	1.32	0.43	138	27
300 nm MoO_3/Cu	1.47	0.32	136	20
400 nm MoO_3/Cu	1.47	0.42	118	13

films, as a function of thickness, are similar pointing out to fixed mechanical properties at 100 nm of film thickness. These results constitute a stimulating hint for the growth of MoO_3 films on copper for technological application, bearing in mind that the coating grip and their mechanical properties can be improved, performing growth at substrate temperature higher than RT.

B. Electronic, structural, and chemical properties: XAS, XRD, Raman spectroscopy, and AES

XAS is a powerful spectroscopic technique that, in addition to the local structure around the photoabsorber, probes the local and partial empty density of states around the excited atom.

The observed prepeak in Fig. 5 is due to the mixing of 2p orbitals of oxygen hybridized with 5p and 4d orbitals of molybdenum. Such mixing occurs for distorted MoO_6 octahedra. The comparison with the reference MoO_3 spectra from Kopachevska *et al.*[26,27] of the XANES spectra of the four samples points out that these coatings are characterized by a strong shoulder at the edge typical of MoO_3.

The subtle changes of the empty density of states showed in the right panel in Fig. 5 indicate a variation in the difference of the occupied electronic levels and of degree of hybridization in these films. The difference spectra of the XANES spectra with respect to the thinnest film (50 nm) show that the local structure is the same, while increasing the thickness, there are changes in the empty density of states of p character that are correlated with the change in the conductivity of these films' growth on metallic copper. The difference spectra shown in Fig. 5 (right) follow the increase of the thickness. A first change occurs for the 100 nm thick film, while for the thicker films the increase of the empty density of states occurs nearer the Fermi energy. These changes could be correlated with the transport properties of these films and to the charge transfer from the substrate, which is larger in the thinner film. Indeed, Cu may act as an n-type dopant for MoO_3. If Cu is oxidized to Cu^+, it reduces Mo^{6+} to Mo^{5+}, donating electrons to the MoO_3 conduction band. This process generates a partially filled Mo 4d-band, but the MoO_3-structure is preserved.[28–30]

About the x-ray diffraction, we measured MoO_3 films with thickness from 50 to 1000 nm. The diffraction patterns showed only characteristic diffraction peaks from polycrystalline copper. This is probably due to the amorphous texture of our MoO_3 films grown at RT.

To clarify this issue, we performed Raman spectroscopy on a series of MoO_3/Cu films of 100, 300, 400, and 500 nm thicknesses, grown at RT on the polycrystalline polished Cu substrate. Figure 6 shows a typical Raman spectrum of an amorphous a-MoO_3 film (100 nm), whereas the inset reports the other higher MoO_3 thicknesses. Three prominent shoulders, indicated by vertical lines, are clearly observed in the wide-ranging spectrum (600–1000 cm^{-1}). There is a broad peak at 829 cm^{-1} due to phonons in the disordered O—Mo^{6+}—O framework and a moderately pronounced shoulder at ~953 cm^{-1}, which has been assigned to the Mo^{6+} =

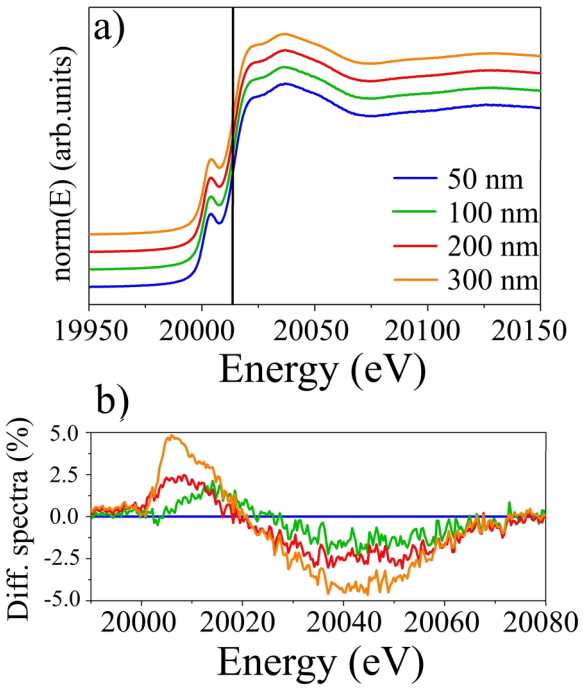

FIG. 5. (a) Mo K-edge XANES spectra from the MoO_3 film of 50, 100, 200, and 300 nm of thickness; the vertical line indicates, for all the curves, the K-edge energy; (b) difference spectra between each spectrum and that of the 50 nm sample, taken as a reference.

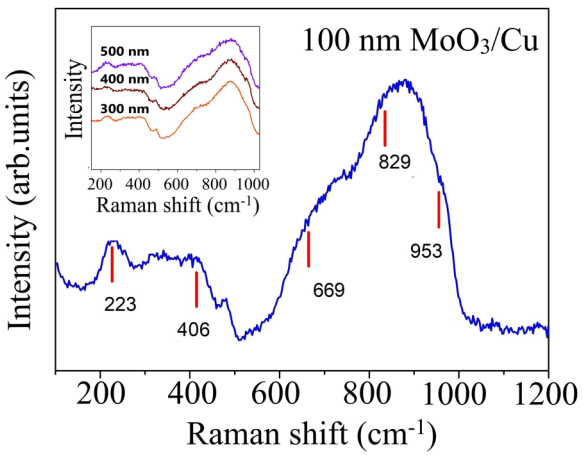

FIG. 6. Raman spectra of the 100 nm amorphous MoO_3 film deposited on the polycrystalline Cu. Inset: Raman spectra of the 300, 400, and 500 nm MoO_3 films.

O stretching mode of terminal oxygen atoms lying on the surface the amorphous film.[15] These oxygen terminal bonds originated by the Mo_2—O bond breaking at the corner-shared oxygen atoms, which are common between two octahedral sites in the α-phase MoO_3.

In addition, a weaker peak is present at 989 cm^{-1}, whose origin comes back to the $Mo^{6+}=O$ stretching mode of terminal oxygen bonds originated from single coordinated oxygen in the α-phase layered MoO_3.[15,31] The broad peak at 220 cm^{-1} is typical of an MoO_3 structure, whereas the peak at ~406 cm^{-1} can be attributed to vibrations of the bonds between Mo^{5+} and oxygen atoms.[31] Here, we note that Raman structures of the thicker MoO_3 (see the inset of Fig. 6) are very similar, pointing out an amorphous configuration for all films.

The chemical composition of the MoO_3 films was probed by Auger spectroscopy. A typical Auger spectrum from the 100 nm thick MoO_3 film is reported in Fig. 7.

The AES spectrum in Fig. 7 shows three Mo main features: $M_{4,5}N_1V$ (160 eV), $M_{4,5}N_{2,3}V$ (182 eV), and $M_{4,5}VV$ (220 eV) transitions, with each one splitting into doublets that are characteristics of the MoO_3 stoichiometry.[32] The Auger peak-to-peak height ratio between the two peaks in the Mo $M_{4,5}N_{2,3}V$ doublet, indicated by the two arrows, larger than one is the fingerprint of Mo^{6+}, having MoO_2 (Mo^{4+}) stoichiometry a ratio smaller than one.[32] In addition to chemical information, the selected Auger decay is extremely important since they all have at least one hole in the conduction band, proving that it is partially filled or that due to defects or oxygen vacancies or Cu substrate dopant action some gap states just below the conduction band are present. This observation is in agreement with the results obtained by Castro *et al.*[19] where the charge transfer from the metal Fermi level in the molybdenum oxide's conduction band results in the reduction of MoO_3. This is an additional proof that the electronic structure of MoO_3 is not that of an insulator as it could be expected in a simple ionic picture and that in this kind of system unique transport properties may be observed.

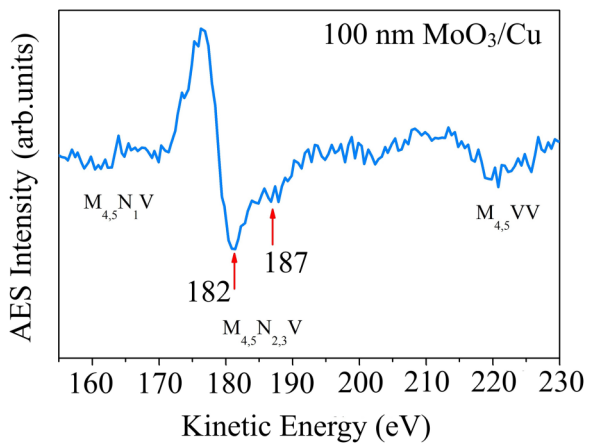

FIG. 7. Mo Auger MNN valence spectrum from the 100 nm MoO_3 film on a polished polycrystalline Cu substrate taken with the beam energy $E_p = 1$ keV. The two arrows indicates the energy of the doublet (181.5 and 187 eV) of the Mo $M_{4,5}N_{2,3}V$ AES transition.

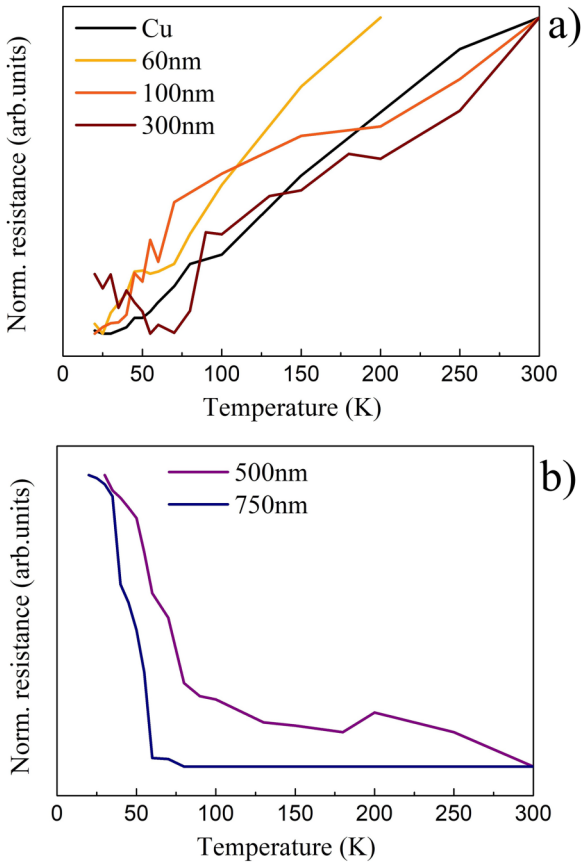

FIG. 8. Normalized electrical resistance as a function of temperature of the Cu substrate and the MoO_3 films of 60, 100, and 300 nm (a) and 500 and 750 nm (b).

C. Transport properties: I–V characteristics and secondary electron spectroscopy for work function measurements

We measured the transversal resistance as a function of the temperature for several MoO_3 films with the thickness ranging from 60 up to 750 nm and compared with that of the copper substrate. Samples were located in an optical cryostat, equipped with a cold finger using a temperature controlled liquid helium continuous flow. The measurements were performed cooling the sample in the temperature range from RT down to 20 K (±10 mK).

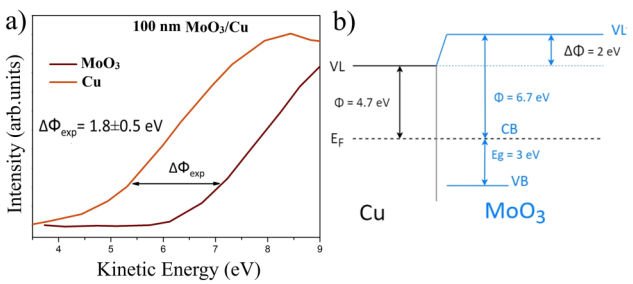

FIG. 9. Secondary electron curves collected on the Cu substrate and on a 100 nm thick MoO_3 film (a). On the right (b), a simplified description of the band structure of the MoO_3/Cu system with the predicted energy gap and the measured WF of both MoO_3 and Cu is shown.

TABLE II. Experimentally measured values of the WF for different metals (Ref. 5).

Element	Φ_m (eV)	Element	Φ_m (eV)	Element	Φ_m (eV)
Sc	3.5 ± 0.15	Ni	5.15 ± 0.1	Ag	4.0 ± 0.15
Ti	4.3 ± 0.1	Cu	4.7 ± 0.05	La	3.5 ± 0.2
V	4.3 ± 0.1	Y	3.1 ± 0.15	Ce	2.9 ± 0.2
Cr	4.5 ± 0.15	Zr	4.05 ± 0.1	Sm	2.7 ± 0.3
Mn	4.1 ± 0.2	Nb	4.3 ± 0.15	Gd	3.1 ± 0.15
Fe	4.5 ± 0.15	Mo	4.6 ± 0.15	Pt	5.65 ± 0.1
Co	5.0 ± 0.1	Pd	5.55 ± 0.1	Au	5.4 ± 0.1

Normalized resistances are shown in Fig. 8 in order to compare the conductive behavior of the samples. Measures clearly show that MoO_3 films with thickness >500 nm have a semiconducting behavior, while for thickness <300 nm a metallic behavior was found, with a conductivity similar to copper.[33]

These results are in good agreement with those reported by Bonavolontà *et al.*,[33] obtained by normal incidence reflectance spectroscopy in the midinfrared range (500–8000 cm^{-1}) at room temperature. Metallic and insulating reflectance was observed for thin and thick MoO_3 films, respectively.[33]

As pointed out in the introduction, secondary electron spectroscopy allows for obtaining the work function of materials. The edge curves of the secondary electron cut for both Cu substrate and 10 nm MoO_3 film are reported in Fig. 9(a), and in Fig. 9(b), we show a simplified model[28] of the band structure of the MoO_3/Cu system with the predicted energy gap and the measured WF value of both MoO_3 and Cu.

This simplified model for the MoO_3/Cu system[34] shown in Fig. 9(b) was obtained by aligning the Fermi energy level of the metal with the conduction band of the oxide. The picture shows that the work function of the film (Φ_{MoO3}) is expected to be 2 eV higher than the Φ_{Cu} value, which is in excellent agreement with our experimental results, where $\Phi_{Cu} = 4.7$ eV and $\Phi_{MoO3} = 6.5$ eV, giving a $\Delta\Phi = 1.8$ eV.

We report in Table II the experimentally measured value of the WF for different metals. As we can see, the metals have characteristic WFs ranging between 2.7 and 5.7 eV. In particular, the WF of copper is ~4.7 eV. Our thin MoO_3 films deposited on copper may have a variable conductivity as a function of temperature, as shown in Fig. 8, and a WF at a room temperature of ~6.5 eV, a value from ~1 up to ~4 eV higher than nominal values reported in Table II for bulk metals. A similar effect, although smaller, has also been observed for MoO_3 evaporated on carbon nanotubes, where a decrease of the resistivity of two orders of magnitude was also measured.[34]

IV. CONCLUSIONS

Molybdenum trioxide films were grown from 30 nm up to 1 μm thickness, on polished polycrystalline Cu substrates at room temperature and investigated with different techniques in order to get insights on their morphological, structural, and electronic properties.

AFM shows the morphology formed by a continuous "bed" of "grainlike" structures with diameter in the 30–100 nm range, and roughness of the order of 3–4 nm as probed by AFM and STM. As for the nanoindentation measurements, the resulting film hardness is comparable to copper.

AES and secondary electron spectroscopy allowed us to measure the work function on our MoO_3 films: $\Phi_{MoO3} = 6.5$ eV, about 1.8 eV higher than that of the copper substrate ($\Delta\Phi = \Phi_{MoO3} - \Phi_{Cu} = 1.8$ eV). Furthermore, MoO_3 films exhibited an amorphous texture, evidenced by the total absence of x-ray diffracted peaks and the presence of typically Raman broad structures related to noncrystalline molybdenum oxide phases. Finally, a different conductivity behavior as a function of temperature down to 20 K was observed. Films ranging from 20 up to 300 nm were metallic, while for higher thickness a semiconducting character was measured, which is in agreement with the changes observed at the Fermi energy of the XANES spectra of these thin films. These findings promote the MoO_3/Cu system as a potential material for reduce dark current and protect from breakdown discharge, very well suitable for technology, e.g., high field radio-frequency cavities and space applications.

ACKNOWLEDGMENTS

This research in cooperation with INFN Laboratori Nazionali di Frascati, CNR-ISM, ARTOV, Roma, INFN Napoli, CNR-ISASI, and Tor Vergata University was developed in the framework of DEMETRA, a project funded by the V Committee of the INFN. Part of this research was performed as in house research program of the Diamond Light Source, the U.K. National Synchrotron Radiation Facility. The authors gratefully acknowledge G. Cappuccio for his invaluable support during XRD measurements.

[1]D. Mcwhan, A. Menth, and J. Remeika, J. de Phys. Col. **32**, C1 (1971).
[2]C. N. R. Rao and A. K. Cheetham, Science **272**, 5260 (1996).
[3]A. J. Freeman and J. J. Yu, Mat. Sci. Forum **37**, 267 (1989).
[4]Z. Y. Wu, D. C. Xian, T. D. Hu, Y. N. Xie, Y. Tao, C. R. Natoli, E. Paris, and A. Marcelli, Phys. Rev. B **70**, 033104 (2004).
[5]P. Wasserscheid and W. Keim, Angew. Chem. Int. Ed. **39**, 3772 (2000).
[6]H. Kim, J. Son, A. Kulkarni, C. Ahn, K. S. Kim, D. Shin, G. Y. Yeom, and T. Kim, Nanotechnology **28**, 175601 (2017).
[7]B. Y. Zhang *et al.*, Adv. Funct. Mater. **28**, 1706006 (2018).
[8]T. Daeneke *et al.*, ACS Nano **11**, 6782 (2017).
[9]E. S. Ramanathan, *Thin Film Metal-Oxides. Fundamentals and Applications in Electronics and Energy* (Springer, 2010).
[10]D. R. Lide, *CRC Handbook of Chemistry and Physics*, 90th ed. (CRC, 2009).
[11]S. Chakraborty, M. K. Bera, G. K. Dalapati, D. Paramanik, S. Varma, P. K. Bose, S. Bhattacharya, and C. K. Maiti, Semicond. Sci. Tech. **21**, 467 (2006).
[12]J. Meyer, S. Hamwi, M. Kröger, W. Kowalsky, T. Riedl, and A. Kahn, Adv. Mater. **24**, 40 (2012).
[13]M. T. Greiner, L. Chai, M. G. Helander, W. Tang, and Z. H. Lu, Adv. Funct. Mater. **22**, 4557 (2013).
[14]S. Han, W. S. Shin, M. Seo, D. Gupta, S. J. Moon, and S. Yoo, Org. Electron. **10**, 791 (2009).
[15]M. Diskus, O. Nilsen, H. Fjellvåg, S. Diplas, P. Beato, C. Harvey, E. S. Lantman, and B. M. Weckhuysen, J. Vac. Sci. Technol. A **30**, 01A107 (2012).
[16]E. D. Hanson, L. Lajaunie, S. Hao, B. D. Myers, F. Shi, A. A. Murthy, C. Wolverton, R. Arenal, and V. P. Dravid, Adv. Funct. Mater. **27**, 1605380 (2017).

[17]Y. Guo and J. Robertson, Appl. Phys. Lett. **105**, 222110 (2014).
[18]R. Naouel, H. Dhaouadi, F. Touati, and N. Gharbi, Nano-Micro Lett. **3**, 4 (2011).
[19]I. A. de Castro, R. S. Datta, J. Z. Ou, A. Castellanos-Gomez, S. Sriram, T. Daeneke, and K. Kalantar-zadeh, Adv. Mat. **29**, 1701619 (2017).
[20]D. O. Scanlon, G. W. Watson, D. J. Payne, G. R. Atkinson, R. G. Egdell, and D. S. L. Law, J. Phys. Chem. C **114**, 10 (2010).
[21]Y. Xu *et al.*, J. Phys. Conf. Ser. **430**, 012091 (2013).
[22]A. Marcelli, B. Spataro, G. Castorina, W. Xu, S. Sarti, F. Monforte, and G. Cibin, Cond. Mat. **2**, 18 (2017).
[23]S. Lagotzky, R. Barday, A. Jankowiak, T. Kamps, C. Klimm, J. Knobloch, G. Müller, B. Senkovskiy, and F. Siewert, Eur. Phys. J. Appl. Phys. **70**, 21301 (2015).
[24]R. Das, M. Deo, J. Mukherjee, and M. S. R. Rao, Surf. Coat. Tech. **353**, 292 (2018).
[25]A. D. Cahill, J. B. Rosenzweig, V. A. Dolgashev, Z. Li, S. G. Tantawi, and S. Weathersby, Phys. Rev. Accel. Beams **21**, 061301 (2018).
[26]N. S. Kopachevska, A. K. Melnyk, I. V. Bacherikova, V. A. Zazhigalov, and K. Wieczorek-Ciurowa, Хімія, фізика та технологія поверхні **6**, 474 (2015).
[27]H. Aritani, T. Tanaka, T. Funabiki, and S. Yoshida, J. Phys. Chem. **100**, 5440 (1996).
[28]M. Kröger, S. Hamwi, J. Meyer, T. Riedl, W. Kowalsky, and A. Kahn, App. Phys. Lett. **95**, 123301 (2009).
[29]T. Ressler, R. E. Jentoft, J. Wienold, M. M. Gu1nter, and O. Timpe, J. Phys. Chem. B **104**, 27 (2000).
[30]A. Marcelli *et al.*, Surf. Coat. Tech. **261** (2015).
[31]S. H. Lee, M. J. Seong, C. E. Tracy, A. Mascrarenhas, J. R. Pitts, and S. K. Deb, Solid State Ionics **147**, 129 (2002).
[32]T. T. Lin and D. Lichtman, J. Vac. Sci. Technol. **15**, 1689 (1978).
[33]C. Bonavolontà *et al.*, "Characterization of the transport properties of MoO_3 films on copper," INFN-17-13/LNF, Laboratori Nazionali di Frascati, Italy (2017).
[34]S. Esconjauregui, L. D'Arsié, Y. Guo, J. Yang, H. Sugime, S. Caneva, C. Cepek, and J. Robertson, ACS Nano **9**, 10 (2015).